Band structure and interband optical transitions in the sawtooth superlattice

V. Milanović
Faculty of Electrical Engineering, Bulevar Revolucije 73, Belgrade, Yugoslavia
and High Technical Post Telegraph and Telephone School, Zdravka Čelara 16, Belgrade, Yugoslavia

Z. Ikonić and D. Tjapkin
Faculty of Electrical Engineering, Bulevar Revolucije 73, Belgrade, Yugoslavia
(Received 21 April 1987)

The band structure and interband matrix elements of the $Al_xGa_{1-x}As$ sawtooth superlattice are analyzed. We have shown that the envelope wave functions may be expressed as integrals of elementary functions. Numerical results are given for a superlattice with maximal mole fraction $x_{max}=0.3$, and period equal to 14 nm. A comparison of our results with those obtained via the pseudopotential method is given. Also, the possibility of determining the conduction-band offset ΔE_c from optical measurements, based on strong dependence of the transition matrix elements on ΔE_c, is discussed.

Multilayer graded-gap sawtooth superlattices have recently attracted great attention. In Ref. 1 F. Capasso *et al.* proposed a photodetector comprising this structure, making use of the fact that electrons and holes are spatially separated. Such a photodetector would have a transient photoinduced voltage response of about 10 mV and a decay time of 200 ps.

Treatment of sawtooth-superlattice band structures has been presented in a few papers, based both on the effective-mass approximation and the pseudopotential approach. In Refs. 2–4 the sawtooth-superlattice band structure was calculated via the pseudopotential method, for transverse wave vector $k_t=0$ only. Brum *et al.*[5] used the effective-mass approximation (with the effective-mass variation itself neglected) to find the band structure and the photovoltaic response of a sawtooth superlattice.

In this paper we shall extend the effective-mass-approximation treatment to include the effects of the effective-mass variation, and proceed to analyze the interband optical absorption in sawtooth superlattice.

The $Al_xGa_{1-x}As$ sawtooth superlattice is a structure with linear variation of Al mole fraction $x(z)=x_{max}(z/d)$ within period d. The graded Al concentration creates a potential which is similar to an external electric field potential, with the difference that it concentrates the carriers on the same side of the heterointerface in both the valence and conduction bands (Fig. 1). Within the effective-mass approximation the envelope-wave-function Schrödinger equation for electrons (and holes) is

$$-\frac{\hbar^2}{2}\frac{d}{dz}\left[\frac{1}{m^*(z)}\frac{d\Psi}{dz}\right]+\left[U_e(z)+\frac{\hbar^2 k_t^2}{2m^*(z)}\right]\Psi=E\Psi\ , \tag{1}$$

where E is the total electron energy and k_t the transverse wave vector. For $x_{max}\leq 0.4$, the direct energy gap in $Al_xGa_{1-x}As$ varies linearly with x, thus U_e varies as αz. As for the $m^*(x)$ dependence, there are two expressions currently used in the literature, the more familiar of which relies on the supposition of a linear effective mass versus alloy composition dependence:[6]

$$m_1^*(x)=m^*_{GaAs}+(m^*_{AlAs}-m^*_{GaAs})x\ , \tag{2}$$

and another that supposes a linear Kane's-matrix element squared versus composition dependence:[7]

$$[m_2^*(x)]^{-1}=(1-x)(m^*_{GaAs})^{-1}+x(m^*_{AlAs})^{-1}\equiv B+Az\ . \tag{2'}$$

Assuming the second expression (2′), and after a lengthy calculation we find that (1) does have a particular solution in analytic form:

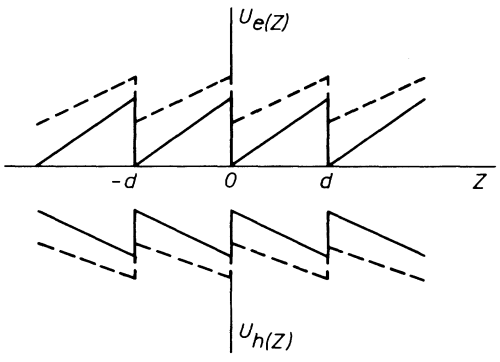

FIG. 1. Conduction- and valence-band profiles in sawtooth superlattice for the transverse wave vector $k_t=0$ (solid lines) and $k_t\neq 0$ (dashed lines).

$$\Psi_{p1}(y)=\int_0^{+\infty}\frac{ch[\sqrt{\varepsilon_2}\,y\,th(s)-(\varepsilon_1/\sqrt{\varepsilon_2})s]}{ch(s)}ds\ ,$$

$$\varepsilon_1\equiv\frac{2}{\hbar^2A^2m_0}(E+\alpha\frac{B}{A}),\quad \varepsilon_2\equiv\frac{2}{\hbar^2A^2m_0^2}\left[\frac{\alpha}{A}+\frac{\hbar^2k_t^2}{2}\right], \tag{3}$$

where m_0 is the free-electron mass, and we also introduce the new variable $y\equiv[m_2^*(x(z))/m_0]^{-1}$. The second linearly independent particular solution $\Psi_{p2}(z)$, is to be determined by a standard method.[8] If we use expression (2), however, it is not possible to find a particular solution in analytic form,[9] and the problem may be solved only numerically.

It is interesting to note that due to the effective potential energy

$$U_{\text{eff}}[U_{\text{eff}}=U_e(z)+\hbar^2k_t^2/(2m^*)]$$

dependence on k_t^2 caused by effective-mass variation, the U_{eff} shape changes and may even reverse the sign of its slope with increasing k_t^2 (Ref. 10). Specifically, if (2′) holds, we find that at a definite value

$$k_{t0}^2=\frac{2\alpha d}{x_{\max}}\frac{m^*_{\text{GaAs}}m^*_{\text{AlAs}}}{m^*_{\text{AlAs}}-m^*_{\text{GaAs}}}\frac{1}{\hbar^2} \tag{4}$$

the U_{eff} becomes position independent. However, in case of $Al_xGa_{1-x}As$ sawtooth superlattices, k_{t0} from (4) has too high a value to make this effect significant in optical absorption not too far from threshold or carrier-concentration evaluation. On the other hand, if one could find a semiconductor alloy having a low α value and strong m^* versus composition dependence, the above effect would be strongly pronounced. We also note that this effect is analogous to well-barrier reversal in rectangular superlattices with increasing k_t (Refs. 10, 11, and 12).

The fundamental solutions of (1) y_1 and y_2 and particular solutions (3) Ψ_{p1} and Ψ_{p2} are linearly related to each other uniquely. Applying the Bloch boundary conditions, we get the dispersion relation $E(\mathbf{k})$:

$$\cos(k_zd)=\frac{1}{2}\left[y_1(d^-)+y_2'(d^-)\frac{m^*(d^+)}{m^*(d^-)}\right], \tag{5}$$

where $m^*(d^+)$ and $m^*(d^-)$ are effective masses in GaAs and $Al_{x_{\max}}Ga_{1-x_{\max}}As$.

Numerical calculations were done for a $Al_xGa_{1-x}As$ sawtooth superlattice with maximal mole fraction $x_{\max}=0.3$ and the superlattice period $d=14$ nm, as in Ref. 3. The spatial dependence of conduction- and valence-band edges are given by[6]

$$U_{0e}(\text{eV})=1.247Q_ex_{\max}\frac{z}{d}\ ,$$

$$U_{0h}(\text{eV})=1.247(1-Q_e)x_{\max}\frac{z}{d}\ , \tag{6}$$

where Q_e is the ratio of the conduction-band discontinuity and the energy-gap difference at the $GaAs/Al_xGa_{1-x}As$ interface. As for the choice of the effective-mass versus mole-fraction dependence [(2) or (2′)], our calculations for a $Al_xGa_{1-x}As$ sawtooth superlattice over a wide range of its parameters show that the results obtained when using (2) or (2′) disagree by no more than a few percent relative to each other, so either expression may be used as convenient. The results given here were obtained using (2′) for effective mass versus mole-fraction dependence.

The data on Q_e vary considerably in the existing literature. In our calculations we took values in the range 0.60–0.85 as reliable, although even the values of 0.57 or 0.97 may be found. We got the best agreement between our results and those obtained via the pseudopotential method for $Q_e=0.85$ (for both electrons and holes). Our calculations of superlattice states at the center of the Brillouin zone give the conduction-band (electron) energies 125, 222, and 307 meV, as compared to 140-, 270-, and 310-meV pseudopotential values. For heavy holes (hh) and light holes (lh) we got the following energies (listed by increasing order): 19 meV (hh), 28 meV (lh), 35 meV (hh), and 60 meV (lh). The pseudopotential calculation[3] gives 9, 29, 34, and 50 meV. By comparing the two, one can see that the agreement is fairly good as well. We do not know whether the first and the third level of Ref. 3 is predominantly heavy-hole-like, and the other two light-hole-like, but comparison indicates that this may be the case.

Therefore, it is interesting to note that this earlier value $Q_e=0.85$, when used in the effective-mass Schrödinger equation, results in better agreement with the pseudopotential method than the more recently measured values of Q_e.

Furthemore, we also analyzed the influence of the effective-mass spatial variation by comparing our results with those obtained with constant effective-mass model.[5] The agreement between these two models is generally very good except for the first electron minizone, where a difference of approximately 10% appears.

Next we calculated the envelope-matrix elements for interband transitions, given by

$$M_{\text{env}}(\mathbf{k})=\int_0^d\Psi_e\Psi_h^*dz\ , \tag{7}$$

with the envelope wave functions Ψ_e and Ψ_h normalized to unity within the superlattice period. By comparing the envelope wave functions obtained via the effective-mass model (this work) and the pseudopotential method (Ref. 3), we found that the agreement is approximately as good for energies, so we believe that the former may be fairly reliably used in calculation of optical-transition matrix elements. The dependence of $|M_{\text{env}}|^2$ for $\mathbf{k}=\mathbf{0}$ on Q_e is given in Fig. 2 for (e-hh) transitions. For higher values of Q_e (~0.85) the transition matrix elements between minizones with the same indices are nearly equal to unity, because electron hole wave functions have very similar forms. With decreasing Q_e these matrix elements also decrease, e.g., $|M_{\text{env}}|^2=0.18$ ($Q_e=0.6$) for the (3-3) transition. In case of transitions between minizones having different indices, however, the opposite is true: $|M_{\text{env}}|^2$ increase with decreasing Q_e. The transition matrix element between the third electron and the first heavy-hole minizone is considerably less than the

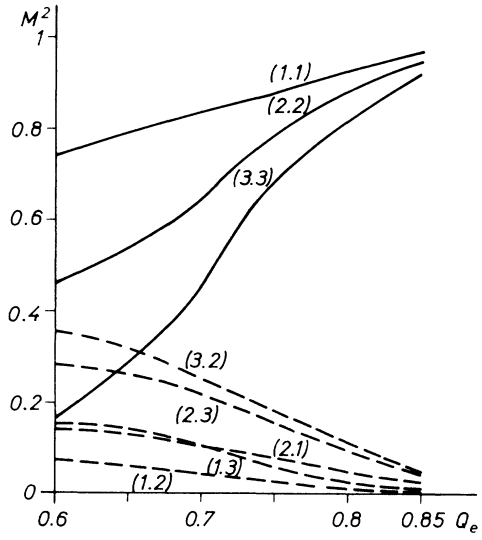

FIG. 2. The electron–heavy-hole transition envelope-matrix elements at $\mathbf{k}=\mathbf{0}$ for sawtooth superlattice with period $d=14$ nm and maximal Al mole fraction $x_{\max}=0.3$. The first number in parentheses is the electron minizone index, and the second is the hole minizone index.

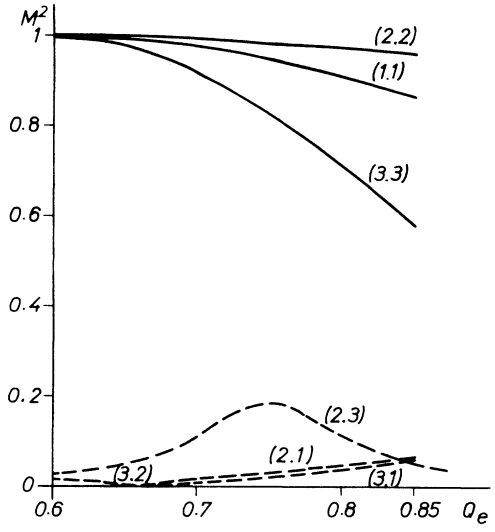

FIG. 3. The electron–light-hole transition envelope-matrix elements at $\mathbf{k}=\mathbf{0}$ for sawtooth superlattice with parameters as in Fig. 2.

others ($|M_{\text{env}}|^2 \leq 0.04$ for all Q_e).

For the electron–light-hole transitions (Fig. 3), the matrix elements connecting minizones of the same index increase with decreasing Q_e, and for $Q_e \leq 0.65$ they are very close to unity, while those for minizones having different indices follow no simple rules. Certainly, because of the lack of inversion symmetry in sawtooth superlattices, there are no parity-forbidden transitions here, as can be seen from Figs. 2 and 3.

Due to the effective-masses position dependence, the wave functions and envelope-matrix elements depend on the transverse wave vector k_t (of electron and hole to be generated by photon absorption). However, for $k_t \ll k_{t0}$ (4), corresponding to photon energies not too far from the absorption threshold, this dependence is only slight, e.g., for (2,2) e-hh transition ($x_{\max}=0.4$, $d=14$ nm) the matrix element is constant within 2% for a photon energy range of 50 meV. The matrix elements vary as k_z varies over the first Brillouin minizone as well. This dependence is very pronounced only for transitions between levels with different indices (matrix elements may change up to 2 orders of magnitude in such cases).

It is well known that the excitonic effects highly influence the absorption spectra of superlattices, especially at threshold.[13,14] To get more realistic values for absorption, the envelope-matrix elements obtained here should be multiplied by $\theta_{eh}(0)$, where the full excitonic wave function Φ is written as

$$\Phi(z_e,z_h,\mathbf{r})=\Psi(z_e)\Psi_h(z_h)\theta_{eh}(\mathbf{r})$$

and $\theta_{eh}(\mathbf{r})$ is to be obtained by variational method.[13,14] These calculations will be performed and presented subsequently. However, the calculated envelope-matrix elements do characterize the superlattice absorption away from the excitonic peaks.

Furthermore, we note that the matrix elements for dominant transitions—(1,1), (2,2), etc. in sawtooth superlattices are rather sensitive functions of Q_e contrary to the case of the conventional "rectangular" superlattices. However, one may expect that the excitonic effects will somewhat decrease their sensitivity on Q_e. Also, the calculated wave functions may be used to determine oscillator strengths of forbidden exciton lines. In conclusion, we may add that the relative oscillator strengths may be used for determination of Q_e, i.e., ΔE_c (those for forbidden exciton lines may prove to be an even better indicator of ΔE_c than interband transitions matrix elements).

The authors would like to thank Professor D. S. Mitrinović for helpful discussions concerning some mathematical aspects of Eq. (1).

[1]F. Capasso, S. Luryi, W. T. Tsang, C. G. Bethea, and B. F. Levine, Phys. Rev. Lett. **51**, 2318 (1983).

[2]M. Jaros, K. B. Wong, and M. A. Gell, J. Vac. Sci. Technol. B **3**, 1051 (1985).

[3]M. Jaros, K. B. Wong, and M. A. Gell, Phys. Rev. B **31**, 1205 (1985).

[4]K. B. Wong, M. A. Gell, D. Ninno, and M. Jaros, Philos. Mag. Lett. **52**, L39 (1985).

[5]J. A. Brum, P. Voisin, and G. Bastard, Phys. Rev. B **33**, 1063 (1986).

[6]H. C. Casey and M. B. Panish, *Heterostructure Lasers* (Academic, New York, 1978).
[7]J. W. Harrison, and J. R. Hauser, J. Appl. Phys. **47**, 292 (1976).
[8]E. Kamke, *Spravochnik Po Obyknovennym Differential'nym Uravneniyam* (Nauka, Moskva, 1973).
[9]D. S. Mitrinović (private communication).
[10]V. Milanović and D. T. Tjapkin, Phys. Status Solidi B **110**, 687 (1982).
[11]R. E. Doezema and H. D. Drew, Phys. Rev. Lett. **57**, 762 (1986).
[12]V. Milanović, D. Tjapkin, and Z. Ikonić, Phys. Rev. B **34**, 7404 (1986).
[13]Y. Kan, M. Yamanishi, Y. Usami, and I. Suemane, IEEE J. Quantum Electron. **22**, 1837 (1986).
[14]J. A. Brum and G. Bastard, Phys. Rev. B **31**, 3893 (1985).